PCCP
Physical Chemistry Chemical Physics

Accepted Manuscript

This article can be cited before page numbers have been issued, to do this please use: B. Durbeej, S. Pinter, A. Hirsch and M. A. Kochman, *Phys. Chem. Chem. Phys.*, 2026, DOI: 10.1039/D6CP01643J.

View Article Online
DOI: 10.1039/D6CP01643J

Journal Name

ARTICLE TYPE

Cite this: DOI: 00.0000/xxxxxxxxxx

UV Photochemistry of the Energy-Storing Isomer of a Norbornadiene-Based Molecular Switch: Ring Opening, Rehybridised Intramolecular Charge Transfer, and Isomerisation into a Carbene Photoproduct†

Bo Durbeej,[a] Simone Pintér,[b] Andreas Hirsch,[b] and Michał Andrzej Kochman*[c]

Received Date
Accepted Date

DOI: 00.0000/xxxxxxxxxx

Photoswitches based on the norbornadiene-quadricyclane (NBD-QC) isomer pair capture solar energy by undergoing the NBD→QC photoisomerisation reaction. The energy-storing QC isomer contains two highly strained three-membered rings, which implies that it may be susceptible to photodegradation through exposure to the ultraviolet (UV) component of sunlight. In the present study, we use nonadiabatic molecular dynamics simulations to investigate the UV-induced photochemistry of the QC isomer of a representative NBD-QC photoswitch with a push-pull substitution motif. A pattern recognition algorithm is employed to analyze and systematize the simulation results. We find that the predominant outcome of UV absorption, observed in 75 out of the 100 simulated trajectories, is the opening of the four-membered ring which belongs to the QC moiety, although in about half of the trajectories which follow this relaxation pathway, the ring promptly closes again. However, in a small fraction of trajectories, the QC moiety instead breaks up, leading to the formation of a carbene photoproduct. We hypothesize that the breakup of the QC moiety is the first step in a reaction pathway which leads to the decomposition of the photoswitch.

1 Background

1.1 Molecular Solar Thermal Energy Storage

The global consumption of energy is increasing at a rate of 1–2% per year.[1] Meeting the rising demand, while at the same time reducing the emissions of greenhouse gases and other forms of pollution, will require developments in technologies which harness renewable energy sources. One emerging sustainable energy technology is molecular solar thermal energy storage (MOST).[2–8] Its underlying principle is the collection, storage, and controlled release of energy from sunlight with the use of photoswitches – materials which can be reversibly converted between two or more states with the use of light. The present study is focused on compounds based on the norbornadiene-quadricyclane (NBD-QC) isomer pair, which include some of the best-performing MOST systems developed so far.[3,9–11] Their operating cycle is shown in Figure 1.

The first half of the cycle consists of the photoisomerisation of the NBD isomer into the QC isomer. In order to increase the photoabsorption coefficient of the NBD isomer in the visible range, atoms C2 and C3 of the NBD moiety are substituted with groups **R2** and **R3** which extend the conjugated π-bonding system. The most successful molecular architecture, and the one with which we will concern ourselves here, is the push-pull substitution pattern, where **R2** is an electron-donating group, and **R3** is an electron-accepting group.[12–22] In order for the NBD isomer to efficiently absorb solar light, a relatively large electron-donating group is required, such as the (4-(dimethylamino)phenyl)ethynyl group found in compound **III**.[12]

The QC isomer acts as the energy-storing form of the photoswitch – due to it having two strained three-membered rings, it is significantly higher in energy than the NBD isomer. Crucially, the QC isomer can be stored for an extended period of time (hours to months, depending on the substitution pattern of the given compound).

In the second half of the operating cycle, the QC isomer is made to revert to the NBD form, releasing the stored energy in the form of heat. The options available for inducing energy release include the use of a catalyst,[23,24] applying an electrochemical

[a] *Division of Theoretical Chemistry, Department of Physics, Chemistry and Biology (IFM), Linköping University, Linköping, Sweden*
[b] *Friedrich-Alexander University of Erlangen-Nuremberg (FAU), Erlangen, Germany*
[c] *Institute of Physical Chemistry, Polish Academy of Sciences (IChF PAN), Warsaw, Poland.* E-mail: mkochman@ichf.edu.pl

† Electronic Supplementary Information (ESI) available: description of benchmark calculations, and setup of NAMD simulations. See DOI: 00.0000/00000000.

View Article Online
DOI: 10.1039/D6CP01643J

Fig. 1 Structure and operating cycle of push-pull NBD-QC photoswitches. Atom numbering in the NBD moiety is shown in red. **I–IV** are representative compounds. Compound **II** is the model system for the purposes of this study.

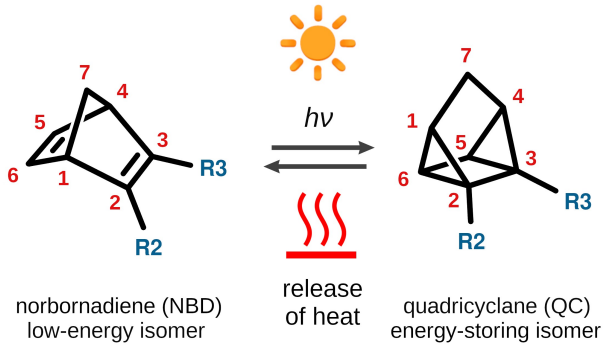

	R2 (donor)	R3 (acceptor)
I	C_6H_5	C≡N
II	C≡C–C_6H_5	C≡N
III	C≡C–*p*-C_6H_4–NMe_2	C≡N
IV	*p*-C_6H_4–NMe_2	CO_2Me

trigger,[24–26] using a redox photocatalyst,[27,28] or, for some compounds, changing the protonation state.[29]

Beginning from the late 2010s, the research group of Moth-Poulsen has constructed prototype MOST devices based on the NBD-QC system[30,31] (see Figure 2 for a schematic illustration) and on some other types of photoswitches: the dihydroazulene-vinylheptafulvene (DHA-VHF) isomer pair[32] and azobenzene.[33] Thus, the technology, and the above-mentioned series of photoswitches in particular, have been successfully demonstrated under laboratory conditions.

1.2 UV Photochemistry of the QC Isomers

The above notwithstanding, there remain major gaps in our understanding of the functioning of the NBD-QC series of photoswitches at the single-molecule level. One specific problem which requires further study is the photochemistry of the energy-storing QC isomer. (A number of studies,[34–39] have examined the mechanism of the NBD→QC photoisomerisation reaction, but the photoinduced reactivity of the QC isomer has not been investigated to the same extent.) In order to introduce the problem, let us refer again to Figure 2. Energy capture (i.e., the NBD→QC photoisomerisation reaction) takes place while the carrier liquid is being passed through the solar collector, and exposed to sunlight. The QC isomer builds up gradually, and it is subjected to sunlight along with the NBD isomer.

For photoswitches with small electron-donating groups, such as **I**, the QC isomer absorbs only the ultraviolet A (UVA) component of sunlight, and then only weakly – the photoabsorption cross section in the UVA range is low. Hence, for these compounds, the photochemistry of the QC isomer can be neglected. Conversely, for some photoswitches with larger donor groups, such as **III** and the compounds reported in Refs. 21 and 22, the absorption spectrum of the QC isomer has more overlap with the solar spectrum. For instance, the QC isomer of **III** in toluene solution shows an intense absorption band in the range 270–330 nm,[12] which falls in the UVA range. Generally speaking, substituents which enhance the absorption of visible light by the NBD isomer also cause a redshift of light absorption by the QC isomer. In these systems, the absorption of light by the QC isomer is inevitable, and its photochemistry will affect the functioning of the device as a whole.

At present, the photoinduced reactivity of the QC isomers is only partially understood. What is known is that the absorption of UV radiation can lead to QC→NBD cycloreversion.[40–42] Interestingly, there is a certain discrepancy in the literature regarding the timescale of that reaction. Alex and co-workers investigated the relaxation process of the QC isomer of **IV** (QC-**IV** for short) following photoexcitation at 258 nm, and reported that cycloreversion occurs over a timescale of ca. 62 ps.[40] However, the relatively long cycloreversion timescale of QC-**IV** seems difficult to reconcile with the findings of a recent study by Borne and co-workers.[41] This latter study characterised the relaxation dynamics of unsubstituted QC (the compound in which **R2** and **R3** are hydrogens) with the use of extreme ultraviolet photoelectron spectroscopy, and with support from computer simulations, notably including nonadiabatic molecular dynamics[43,44] (NAMD) based on rotated multi-state complete active space second-order perturbation theory[45] (RMS-CASPT2). These authors reported a cycloreversion timescale on the order of hundreds of femtoseconds[41] – shorter by two orders of magnitude than the one given in Ref. 40. (NB: with regard to the experimental setup used in Ref. 41, "extreme ultraviolet" refers to the probe pulse, which had a wavelength of 65.35 nm.[41] The pump pulse had a wavelength of 200.6 nm,[41] which falls in the UVC range.)

Leaving aside the question of timescale, the photoinduced QC→NBD cycloreversion reaction returns the photoswitch to the low-energy form, but it is otherwise harmless. Because of the strained structure of the QC isomer, it seems likely that QC→NBD cycloreversion may be accompanied by other photoisomerisation reactions, some of which may be irreversible, and may lead to the decomposition of the photoswitch. Of course, any such reactions would be undesirable, as they would deplete the MOST material of the photoswitch, thus reducing its energy storage capacity. Tellingly, unsubstituted QC does undergo photoinduced fragmentation, in addition to cycloreversion.[41] Moreover, some other compounds with three-membered rings, such as cyclopropane, oxirane, and their derivatives, undergo various photoisomerisation reactions which involve the strained ring.[46–48] This supports the hypothesis that the QC isomers of

View Article Online
DOI: 10.1039/D6CP01643J

Fig. 2 Simplified diagram of a MOST device based on the NBD-QC system, used for the heating of water. The photoswitch is dissolved in a carrier liquid, which is cycled through the device as indicated by arrows. The NBD vs QC composition of the carrier liquid is depicted with the use of color.

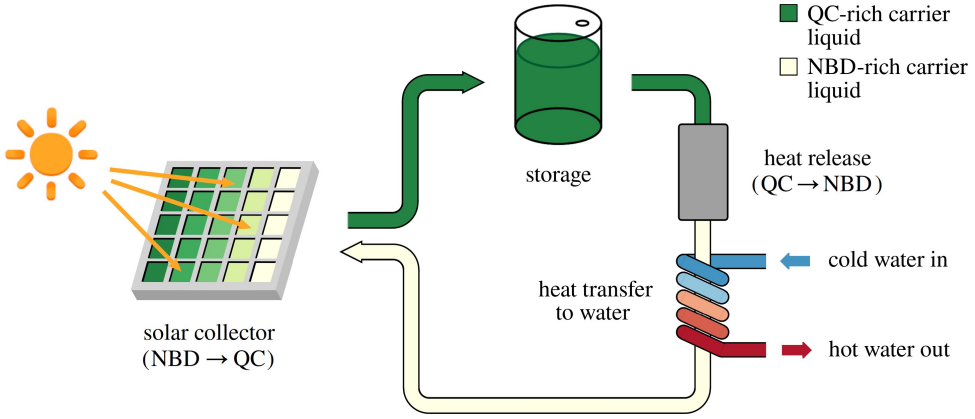

push-pull NBD-QC photoswitches may likewise be susceptible to photoinduced damage.

Further on the subject of photodegradation, Fei and co-workers[42] have tested the photostability of some typical push-pull NBD-QC photoswitches by cycling them between the NBD and the QC forms through alternating irradiation at 365 nm (in order to induce NBD→QC cycloaddition) and at 265 nm (to induce QC→NBD cycloreversion). It was found that the compounds under study underwent photodegradation by oligomerisation.[42] Interestingly, the rate of photodegradation was considerably higher for compounds in which the electron-accepting group is an ester group than for the compound in which it is a nitrile group.[42]

In view of the limited understanding of the photochemistry of the QC isomers, our goal in this study was to gain more insight into their photorelaxation processes, especially with regard to reaction timescales and the photostability of the material. To this end, we here report computer simulations performed to obtain such insight. The rest of the manuscript is organised as follows. In the next section, we outline the simulation methodology. We then move on to examine the simulation results, firstly by identifying the emergent relaxation pathways, and then by examining each such pathway one by one. We conclude with a discussion of how our findings relate to the available experimental data, and how the photoproduct that is predicted by our simulations might potentially be detected and identified experimentally.

2 Computational Methods

2.1 Overview

For the sake of brevity, the main body of this paper only includes a short outline of the simulation setup. The detailed description of the computational methodology, as well as the benchmark calculations which were performed to validate it, is included in the Supplementary Information.

Our approach was to model and analyze the photorelaxation process of the QC isomer of **II** (QC-**II** for short), which can be seen as a representative push-pull NBD-QC photoswitch. The photochemistry of **II** was characterised experimentally in Ref. 12, and its NBD→QC photoisomerisation reaction was already studied computationally in Ref. 38. Note that QC-**II** itself shows only relatively weak absorption in the UVA range.[12] In the present study, it is intended to serve as a computational model of the QC isomers of photoswitches with larger electron-donating groups, which absorb UVA light much more efficiently. We expect that the simulation results can be generalised (in a qualitative sense) to other photoswitches of the same class, though the exact reaction timescales, and the relative importance of different reaction pathways, will no doubt vary from one compound to another.

Because the model system is a single, isolated molecule of QC-**II**, the simulations only provide information on intramolecular reactions. Intermolecular reactions, such as the photoinduced oligomerisation mentioned previously,[42] are not accounted for.

During the course of this study, the photorelaxation mechanism of the QC-**II** turned out to be complex in nature, with multiple reaction pathways leading to different outcomes. For this reason, we devised a pattern recognition algorithm in order to analyze the simulation results.

2.2 Electronic Structure Calculations

The photorelaxation dynamics of QC-**II** was modeled with the fewest switches surface hopping[49–52] (FSSH) variant of the NAMD method. As explained in the next section, NAMD simulations involve on-the-fly calculations of the ground- and excited-state potential energy surfaces (PESs) of the system under study, their gradients, as well as nonadiabatic coupling vectors (NACVs) between the electronic states of interest. Because these quantities must be calculated at each time step of every simulated trajectory, a compromise has to be struck between accuracy and computational efficiency.

In Ref. 38, which focused on the mechanism of NBD→QC photoisomerisation, the electronic structure of the photoswitch was treated using spin-flip time-dependent density functional theory[53–58] (SF-TDDFT). However, even though SF-TDDFT

View Article Online
DOI: 10.1039/D6CP01643J

performed satisfactorily in simulations of NBD→QC photoisomerisation, it is ill-suited to modeling the photochemistry of the QC isomer. This is because the high-spin triplet reference state of SF-TDDFT is numerically unstable at QC-like molecular geometries.[38] (The occurrence of instabilities in the triplet reference state appears to be a general problem with spin-flip methods, and it has been discussed in more detail in Refs. 59 and 60.) In the NAMD simulations reported in Ref. 38, the numerical instabilities manifested themselves as an upward drift in the total energy. When modeling NBD→QC photoisomerisation, this effect was less of an issue, because it only came into play at the final stage of the simulation – after the molecule had undergone photoisomerisation into the QC form. Conversely, when modeling the relaxation dynamics of the QC isomer, the problem would appear from the very start of the simulation.

Due to the above considerations, in the present study we used instead another non-standard variant of TDDFT: the TDDFT plus one double (TDDFT-1D) method of Teh, Subotnik, and co-workers.[61–64] TDDFT-1D can be seen as an ad hoc modification of the configuration interaction singles (CIS) method; the electronic states of the system are obtained through the diagonalisation of the following Hamiltonian:

$$\mathbf{H} = \begin{bmatrix} \langle \Psi_0 | H | \Psi_0 \rangle & 0 & \langle \Psi_0 | H | \Psi^{l\bar{l}}_{h\bar{h}} \rangle \\ 0 & \langle \Psi^a_i | H | \Psi^a_i \rangle & \langle \Psi^a_i | H | \Psi^{l\bar{l}}_{h\bar{h}} \rangle \\ \langle \Psi^{l\bar{l}}_{h\bar{h}} | H | \Psi_0 \rangle & \langle \Psi^{l\bar{l}}_{h\bar{h}} | H | \Psi^a_i \rangle & \langle \Psi^{l\bar{l}}_{h\bar{h}} | H | \Psi^{l\bar{l}}_{h\bar{h}} \rangle \end{bmatrix} \quad (1)$$

Here, Ψ_0 is the Kohn-Sham ground-state determinant. Ψ^a_i denotes singly excited configuration state functions in which one electron has been excited from occupied orbital i to virtual orbital a. Note that the matrix elements between Ψ_0 and the singly excited configuration state functions are zero according to Brillouin's theorem. Lastly, $\Psi^{l\bar{l}}_{h\bar{h}}$ is a special doubly excited configuration which corresponds to the excitation of two electrons from occupied orbital h to virtual orbital l, where the orbitals h and l are constructed in such a way as to minimise the energy of this configuration.

Importantly, Teh and Subotnik have shown that TDDFT-1D can predict the correct (conical) topology of crossings between the lowest singlet excited state (S_1) and the singlet ground state (S_0).[61] Furthermore, analytic expressions for TDDFT-1D gradients and NACVs have been derived by Athavale and co-workers.[64]

At present, TDDFT-1D is limited to singlet states. For this reason, our simulations do not account for the possibility of intersystem crossing (ISC) into the triplet manifold. Because the spectroscopic study of Alex et al.[40] did not observe ISC during the photorelaxation dynamics of QC-**IV**, we believe that the neglect of ISC is a justified approximation for QC-**II**.

The TDDFT-1D calculations were performed with the electronic structure software package Q-Chem[65,66] (version 6.3), which is currently the only program implementing that method. The CAM-B3LYP functional[67] was employed in combination with the def2-SV(P) basis set.[68] Lacking diffuse basis functions, the relatively small def2-SV(P) basis set is unable to describe diffuse (Rydberg-type) excited states. This is acceptable for our purposes because, in the real system, the presence of solvent molecules will presumably destabilize the diffuse excited states of the photoswitch relative to the valence excited states. This effect has previously been demonstrated for other organic chromophores.[69] Hence, diffuse excited states are not expected to play a role in the photochemistry of **II** or other push-pull NBD-QC photoswitches in the solution phase.

Because TDDFT-1D is a relatively new and untested method, we assessed its accuracy for the ground- and excited-state PESs of push-pull NBD-QC photoswitches. This was done by benchmarking against the extended multi-state complete active space second-order perturbation theory[70] (XMS-CASPT2). The description of these calculations is provided in the Supplementary Information. Encouragingly, we found reasonably close agreement between the PESs predicted by TDDFT-1D and XMS-CASPT2. This suggests that TDDFT-1D provides a realistic description of the relevant PESs of push-pull NBD-QC photoswitches.

2.3 Nonadiabatic Molecular Dynamics Simulations

Within the framework of NAMD, the nuclear wavepacket of the system is approximated as a set of mutually independent semiclassical trajectories, $\{\mathbf{R}(t)\}$. In each such trajectory, $\mathbf{R}_i = \mathbf{R}_i(t)$, the motions of the nuclei are described with the use of classical dynamics. Meanwhile, the electronic wave function of the system is taken into account explicitly with the use of on-the-fly electronic structure calculations. More specifically, the electronic wave function of the system in each trajectory is expressed as a linear combination of adiabatic states $\{\psi(\mathbf{r};\mathbf{R}_i)\}$ with time-dependent complex coefficients $\{a_j(t)\}$:

$$\Psi(\mathbf{r},t;\mathbf{R}_i) = \sum_j a_j(t)\, \psi_j(\mathbf{r};\mathbf{R}_i) \quad (2)$$

The time evolution of the expansion coefficients is governed by the following system of equations:

$$\mathrm{i}\hbar\, \dot{a}_k = \sum_j a_j(t) \left(\delta_{kj}\, E_k(\mathbf{R}_i) - \mathrm{i}\hbar\, \dot{\mathbf{R}}_i \cdot \mathbf{d}_{kj}(\mathbf{R}_i) \right) \quad (3)$$

where δ_{kj} denotes the Kronecker delta, $E_k(\mathbf{R})$ is the PES of the k-th state, and $\mathbf{d}_{kj}(\mathbf{R})$ is the NACV between states k and j:

$$\mathbf{d}_{kj}(\mathbf{R}) = \langle\, \psi_k(\mathbf{r};\mathbf{R}) \,|\, \nabla_{\mathbf{R}} \,|\, \psi_j(\mathbf{r};\mathbf{R}) \,\rangle \quad (4)$$

In the FSSH scheme, at any given time, one state from among those included in the linear expansion 2 is singled out as the occupied, or current, state in the given trajectory. The dynamics of the nuclei is propagated according to the classical equations of motion on the PES of that state. Nonadiabatic effects are accounted for by allowing the trajectory to undergo a switch (or, "hop") from the current state into another state from among those included in the linear expansion 2, which then becomes the new current state for the given trajectory. The switches are imposed stochastically according to the criterion proposed by Tully.[50]

The global picture of state populations in the ensemble of simulated trajectories is conventionally described in terms

View Article Online
DOI: 10.1039/D6CP01643J

of the so-called classical populations. Namely, the classical population $P_j(t)$ of the j-th state is defined as the fraction of trajectories currently occupying that state:

$$P_j(t) = \frac{N_j(t)}{N_{\text{trajs}}} \tag{5}$$

Here, N_{trajs} is the number of simulated trajectories.

In the present case, we set up the initial conditions for the NAMD simulations in such a way as to model the irradiation of QC-**II** near the origin of its first photoabsorption band. We propagated $N_{\text{trajs}} = 100$ trajectories for a period of 750 fs. The linear expansion 2 included the lowest three singlet states of the molecule (S_0 to S_2). We note here that the relatively low number of simulated trajectories and short simulation time preclude the calculation of photoisomerisation quantum yields. Above all, the simulation time is too short to capture possible isomerisation reactions taking place in the hot ground state. This is nevertheless acceptable for our purposes, as we are mainly aiming for a qualitative insight into the behaviour of the model system, rather than quantitative data. At the same time, we cannot rule out the possibility that our simulations failed to detect some unknown relaxation pathways that are characterised by very low quantum yields. These hypothetical low-yield pathways might potentially be revealed by propagating more trajectories.

Because the number of trajectories is finite, the calculated classical populations are subject to statistical uncertainty. The level uncertainty was estimated by calculating the confidence intervals at a 95% confidence level. To that end, we used the method of Wilson, also known as the Wilson score interval.[71,72]

On the technical side, the simulations were performed with the use of an in-house "wrapper" program, which contains an interface to Q-Chem. More details on our implementation of NAMD are provided in the Supporting Information. The source code of the wrapper program is included as part of the dataset which accompanies our paper.[73]

According to our simulations, the opening and re-closing of the ring formed by atoms C2, C3, C5, and C6 (see Figure 1 for atom numbering) plays an important role in the photochemistry of the QC isomer. In order to monitor that process, we calculated values of parameter $\bar{R}$, which we define as the average of the C2–C6 and the C3–C5 distances. (The interatomic distances which correspond to the bonds being cleaved and reformed.)

$$\bar{R} = \frac{1}{2}\left[R(\text{C2–C6}) + R(\text{C3–C5})\right] \tag{6}$$

We consider $\bar{R} = 1.8$ Å as the threshold value for ring opening. This is because, in Ref. 38, this value was found to be a good threshold for ring *closing*, in the sense that all simulated trajectories which crossed the 1.8 Å threshold went on to form the closed-ring QC isomer. Note that the pattern recognition analysis (see the following section) does not rely on the $\bar{R} = 1.8$ Å criterion to identify ring opening. Instead, it uses a more global representation of molecular geometry.

2.4 Pattern Recognition Analysis

As will be discussed later on, the simulated trajectories followed a number of relaxation pathways. In order to help us analyze the simulation results, we designed a simple pattern recognition algorithm. Its functioning was as follows. For the purposes of the algorithm, each trajectory $\mathbf{R}_i(t)$ was represented by a curve $\widetilde{\mathbf{R}}_i(t)$ whose components are the inverse distances between all pairs of nuclei in the molecule:

$$\widetilde{\mathbf{R}}_i(t) = \left[\frac{1}{|\mathbf{R}_{i,1}(t) - \mathbf{R}_{i,2}(t)|}, \frac{1}{|\mathbf{R}_{i,1}(t) - \mathbf{R}_{i,3}(t)|}, \cdots, \frac{1}{|\mathbf{R}_{i,N-1}(t) - \mathbf{R}_{i,N}(t)|} \right] \tag{7}$$

Here, N is the number of atoms, and $\mathbf{R}_{i,k}(t)$ denotes the position of the k-th nucleus in the i-th trajectory at time t. This representation of a trajectory is loosely based on the Coulomb matrix molecular representation of Rupp and co-workers.[74,75] However, unlike the Coulomb matrix, the representation defined by eq. 7 does not take into account the atomic numbers of the nuclei. This is so as not to bias the algorithm towards atoms of heavier elements. Another point of note is that this representation of the trajectory is solely based on the *nuclear* trajectory; the electronic state of the molecule is not taken into consideration.

The degree of similarity between every pair i and j of representations of trajectories was quantified with the dynamic time warping[76,77] (DTW) algorithm. This procedure yields a diagonal distance matrix $\mathbf{D}$. Each of its elements $D_{ij} = d_{\text{DTW}}(\widetilde{\mathbf{R}}_i(t), \widetilde{\mathbf{R}}_j(t))$ provides an indication of how closely trajectories i and j resemble one another. The calculation of the DTW distance was performed with the similarity_measures Python 3 package, version 1.4.0.[78,79] The resulting distance matrix was rescaled linearly such that its maximum element is 1.

Finally, hierarchical clustering was carried out on the basis of the distance matrix. To that end, we employed Ward's method,[80,81] which is a variant of agglomerative hierarchical clustering. We used the implementation provided in the SciPy package, version 1.11.4.[82] The clustering was visualised in the form of a dendrogram, which can be interpreted as the simulated trajectories being grouped into distinct relaxation pathways.

As explained above, the algorithm works by comparing trajectories, or more accurately, the representations of trajectories. Thereby, it becomes pertinent to asssess how many trajectories are required for the algorithm to produce informative results. We address this issue in Section S3 of the Supporting Information. In brief, the algorithm appears robust with respect to changes in the sample size, and a sample of 100 trajectories is large enough to produce useful results.

3 Results and Discussion

3.1 Pattern Recognition Analysis

In order to set the stage for the subsequent, more detailed discussion of the simulation results, let us begin by reviewing the classification of the individual trajectories into relaxation

View Article Online
DOI: 10.1039/D6CP01643J

pathways. As an illustration of the inner workings of our pattern recognition algorithm, Figure 3 shows the DTW distance matrix **D** between pairs of representations of trajectories. One feature of the distance matrix is readily apparent: there is a subset of around 9 trajectories which are somewhat similar to each other, but highly dissimilar to all other trajectories; the rows and columns which correspond to these 9 or so trajectories are largely colored in orange to red. Actually, it is difficult to determine the exact number of trajectories of this type simply by inspecting the distance matrix, but more important than their number is that they appear at all – they correspond to a distinct relaxation pathway in which the molecule behaves quite differently than in the other trajectories. We will discuss this conspicuous subset of trajectories later on.

The final result of the pattern recognition analysis is the dendrogram which depicts the classification of trajectories, shown in Figure 4. Agglomerative clustering algorithms (such as the method introduced by Ward, which we use here) initially consider each object as its own cluster, and then successively merge clusters according to a certain criterion, until all objects end up in the same cluster. A certain ambiguity arises as to how to determine the optimal number of clusters which best describes the data – informally speaking, when to stop the clustering procedure. In the present case, we inspected the results obtained when the clustering was stopped with between two and seven clusters remaining. We found that at least four clusters are needed to adequately describe the data. When only two or three clusters are retained, trajectories which are markedly dissimilar are grouped together, and so two or three are not enough. With four or more clusters, the classification becomes much more informative. However, when more than four clusters are retained, the clustering becomes overly focused on small differences between trajectories, and that complicates the picture.

On the basis of the above reasoning, we decided to retain four clusters. In order of decreasing size, the four clusters are as follows:

1. The largest cluster contains 41 trajectories whose common feature is that the molecule underwent QC$\rightarrow$NBD cycloreversion, and the ring remained open for the remainder of the simulation.

2. The second-largest cluster consists of 34 trajectories. Here, the molecule also underwent ring opening, but one or both of the broken bonds (i.e., the C2–C6 and C3–C5 bonds) later recombined again.

3. The third cluster comprises 16 trajectories in which the molecule adopted a rehybridised intramolecular charge transfer (RICT) structure.

4. The fourth and smallest cluster contains 9 trajectories in which the QC moiety partially broke up. This is the subset of "around 9" anomalous trajectories which we pointed out earlier, when discussing the structure of the DTW distance matrix.

In order to tie in this classification of trajectories with the dynamics of the molecule, Figure 5 shows three snapshots from one randomly chosen trajectory from each cluster. We will now discuss the various relaxation pathways in more detail, beginning with the ring dynamics (the relaxation pathways which correspond to clusters 1 and 2), and then moving on to the minor relaxation pathways (clusters 3 and 4).

3.2 Main Relaxation Pathways

In this section, we focus on the two relaxation pathways which are statistically dominant, and which mainly involve the opening and, in one of the two, the re-closing of the four-membered ring. For the time being, we neglect the two minor relaxation pathways. Figure 6 (a) shows the classical populations of states S_0 to S_2 in the ensemble of simulated trajectories, while Figure 6 (b) characterizes the ring dynamics by showing values of parameter $\bar{R}$. (Note that this Figure represents data from all 100 simulated trajectories, and not only those which follow the main relaxation pathways.) Complementing our narrative, in the Supplementary Information we include animations of 16 representative simulated trajectories. Animations of the remaining trajectories are available for download from the Zenodo repository as Ref. 73.

The start of the simulation at $t = 0$ corresponds to the initial photoexcitation. As can be seen in Figure 6 (a), the photoexcitation mainly populated state S_1, which was the initially occupied state in 98 out of the 100 simulated trajectories. In the remaining 2 trajectories, the initially occupied state was S_2. During the initial period of roughly 150 fs, there was some exchange of population between states S_1 and S_2, such that the classical population of state S_2 fluctuated around roughly 0.1. (That is to say, individual trajectories hopped back and forth between states S_1 and S_2.) At later times, state S_2 gradually became depleted by internal conversion into states S_0 and S_1, such that its classical population decayed to near zero.

Internal conversion from the excited states (S_1 and S_2) into the ground state began to occur at around $t = 50$ fs. It proceeded at a rapid pace until around $t = 400$ fs, at which point the classical population of state S_0 stabilised at around 0.8, and remained near this value until the end of the simulation at $t = 750$ fs. Meanwhile, the classical population of state S_1 stabilised at around 0.2. Note that the classical populations of all states are subject to statistical uncertainty, but it is still evident that the population of state S_1 is roughly stable from around $t = 400$ fs. The reason that state S_1 was not completely depopulated is because a fraction of the excited-state population became trapped in the RICT state; we will return to this point later on, when discussing the minor relaxation pathways.

The time-evolution of the state populations can be correlated with the ring dynamics, which is characterised in Figure 6 (b). In the majority of trajectories, the C2–C6 and C3–C5 bonds dissociated during the initial 50 fs-long period of time initially following photoexcitation. This resulted in the opening of the four-membered ring, and the formation of the NBD isomer of the photoswitch (denoted NBD-**II**). Interestingly, in most of the trajectories where ring opening took place, it occurred in state S_1 or S_2, without internal conversion to state S_0. As a result,

View Article Online
DOI: 10.1039/D6CP01643J

Fig. 3 DTW distance matrix **D** between representations of trajectories. The individual trajectories are numbered 0001 to 0100. The DTW distance d_{DTW} between each pair of representations of trajectories is indicated with the use of color. Blue to green means close similarity, while orange to red means dissimilarity.

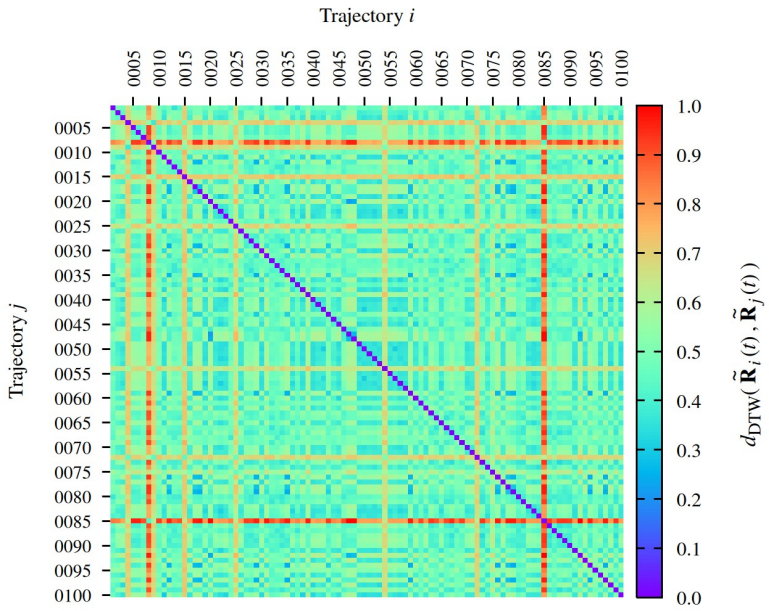

Fig. 4 Dendrogram showing the clustering of trajectories. The clustering was performed on the basis of the DTW distance matrix shown in Figure 3, which is, in turn, based on the time-evolution of molecular geometry in each trajectory.

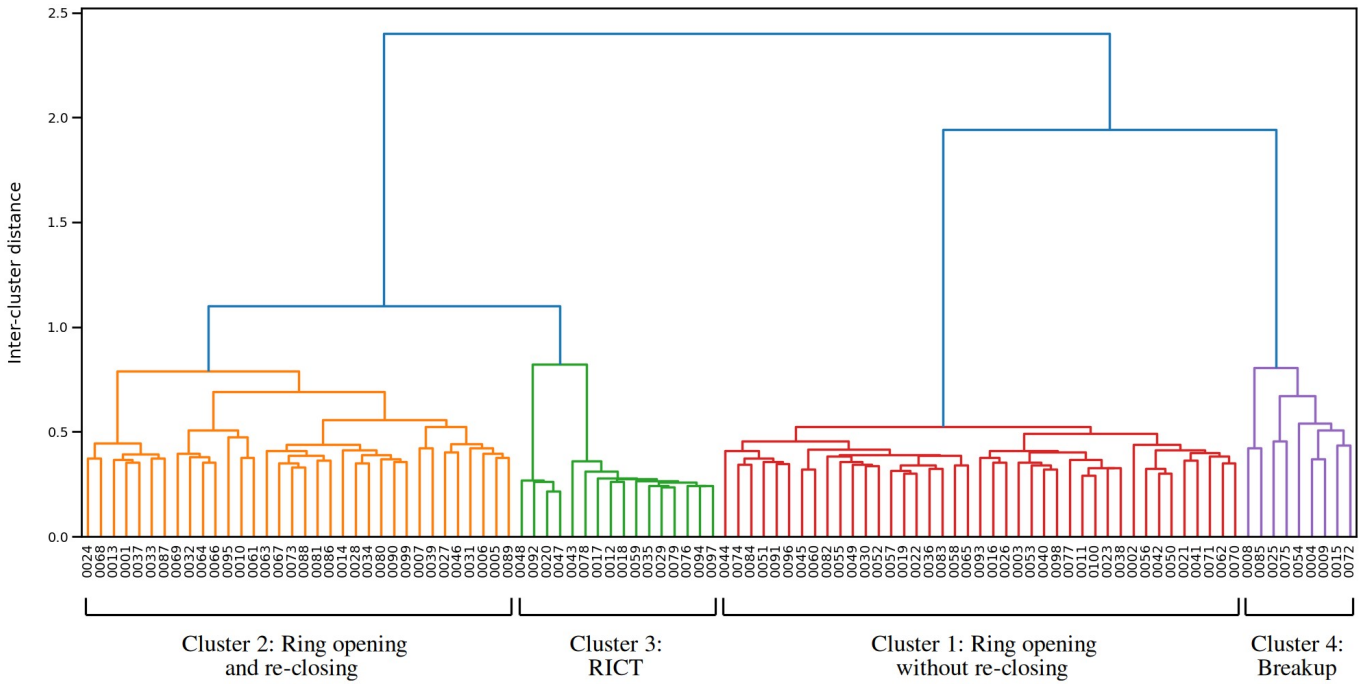

NBD-**II** was formed in an excited electronic state (S_1 or S_2). This is despite the fact that there exists a conical intersection (CI) seam between states S_1 and S_0 which could potentially mediate internal conversion to S_0 while the molecule is undergoing ring opening.[38] More specifically, according to the mixed-reference SF-TDDFT (MRSF-TDDFT) calculations reported in Ref. 38, the minimum-energy geometry along the CI seam – the MECI – is found at R(C2–C3) = 1.972 Å and R(C5–C6) = 1.961 Å.

In order to explain why ring opening took place predominatly without internal conversion to state S_0, let us refer to Figure 7 (a), which shows a schematic diagram of the PESs of states S_1 and S_0. Here, Q_1 represents the reaction coordinate for the interconversion between the NBD-**II** and QC-**II**. It leads from the ground-state geometry of the NBD-**II**, through the S_1/S_0 CI seam, and to the ground-state geometry of the QC-**II**. Q_2 is another internal coordinate that is orthogonal to Q_1. We assume that

View Article Online
DOI: 10.1039/D6CP01643J

Fig. 5 Snapshots from one representative trajectory belonging to each cluster. The first snapshot is taken $t = 0$, and the subsequent two snapshots are taken at intervals of either 100 or 150 fs. The arrows indicate the motions of the nuclei during the corresponding photoisomerisation reaction.

(a) Cluster 1: Ring opening without re-closing

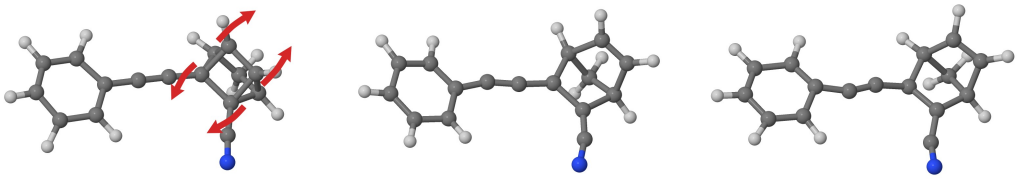

0 fs 100 fs 200 fs

(b) Cluster 2: Ring opening and re-closing

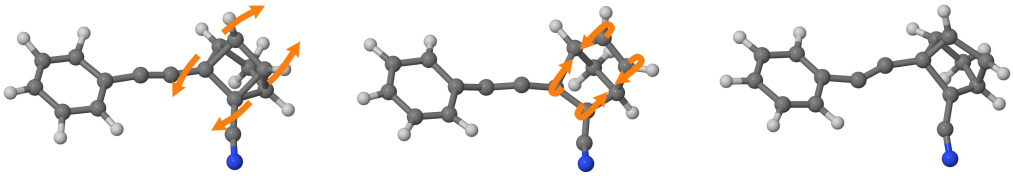

0 fs 100 fs 200 fs

(c) Cluster 3: RICT

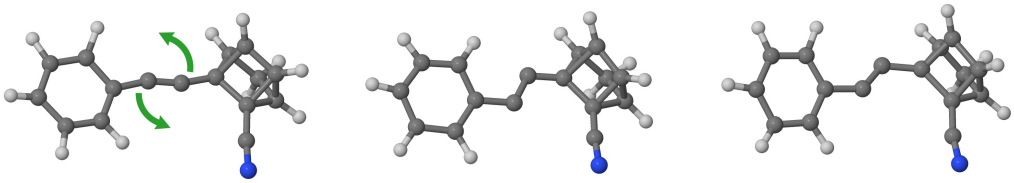

0 fs 150 fs 300 fs

(d) Cluster 4: Breakup

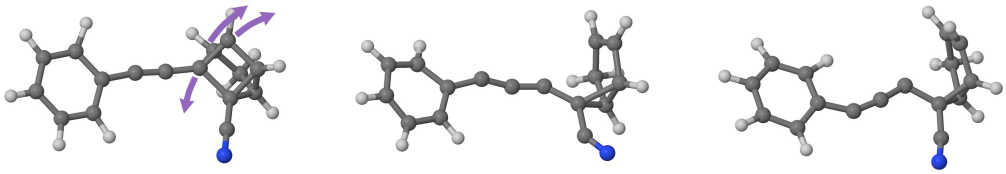

0 fs 150 fs 300 fs

Q_1 and Q_2 both have non-zero components along the branching space vectors of the CI, such that the degeneracy is lifted by motion along Q_1 and/or along Q_2.

As mentioned already, the photoexcitation of the QC-**II** mainly populated state S_1. In the Franck-Condon region, the PES of that state has a steep slope along the reaction coordinate Q_1, which drives the system downward, in the direction of NBD-**II**. The majority of trajectories which evolved along coordinate Q_1 bypassed the S_1/S_0 CI seam. These trajectories reached NBD-like geometries while occupying state S_1 (or occasionally S_2). Afterwards, they were reflected back along the reaction coordinate, and they subsequently approached the S_1/S_0 CI seam from the direction of NBD-**II**. In Figure 7 (a), this sequence of events is labeled **A**.

In about half of the trajectories which encountered the CI seam in this manner, the C2–C6 bond and/or the C3–C5 bonds recombined, which amounts to a re-closing of the ring. In the other trajectories, the bonds failed to recombine, and the ring did not re-close. This is the main feature which distinguishes the trajectories in clusters 1 and 2.

The bypassing of the CI seam during the descent from the Franck-Condon geometry on the PES of state S_1 was also predicted in the joint spectroscopic and computational study by Borne et al,[41] where the photorelaxation dynamics of unsubstituted QC was modeled at the RMS-CASPT2 level. This suggests that it is a common feature of the photochemistry of QC

View Article Online
DOI: 10.1039/D6CP01643J

Fig. 6 Time-evolution of electronic structure (panel (a)) and the geometry of the NBD/QC moiety (panel (b)) during the NAMD simulations. In panel (a), the shaded areas represent the confidence intervals at the 95% level. In panel (b), the horizontal dashed line indicates an $\overline{R}$ value of 1.8 Å, which we consider as the threshold for ring opening. The point when a trajectory hops into state S_0 for the first time is marked with a red dot. NB: this Figure represents data from all 100 simulated trajectories.

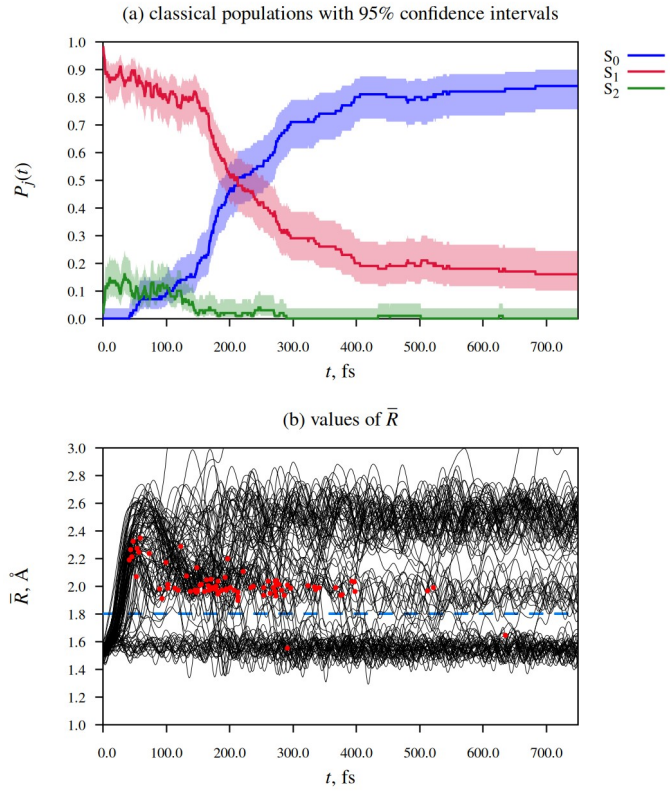

as well as its derivatives.

A few trajectories approached the S_1/S_0 CI seam already during their initial descent from the Franck-Condon region. In this case, the molecule usually hopped down into state S_0 while it was undergoing ring opening. In Figure 7 (a), this relaxation process is labeled **B**.

The mechanism of photoinduced cycloreversion can be compared to the case of photoinduced cycloaddition, which is depicted in Figure 7 (b). In the simulations performed in Ref. 38, during ring closing the molecule always passed through the vicinity of the S_1/S_0 CI seam, where it underwent a hop into state S_0. It seems that the region of the S_1 PES on which the molecule evolves during ring closing steers it towards the CI seam. In contrast, the region of the S_1 PES which the molecule crosses during ring opening apparently causes the molecule to veer away from the CI seam. It follows that the mechanism of photoinduced cycloreversion cannot be fully understood in terms of only a single reaction coordinate Q_1; it is necessary to also take into account motions along an orthogonal reaction coordinate Q_2, which controls whether or not the molecule encounters the CI seam while it is moving along Q_1.

Fig. 7 Comparison of the (a) QC→NBD and (b) NBD→QC photoisomerisation mechanisms of **II**. The graphics show a schematic, qualitative representation of the PESs of states S_0 and S_1 informed by (but not directly based on) the simulation results – a cartoon, so to speak. For the sake of clarity, excited states above S_1 are omitted from this diagram. Q_1 is the reaction coordinate for photoisomerisation, while Q_2 represents an orthogonal internal coordinate. The motions of the nuclear wavepacket are depicted with green arrows. The line segments which would otherwise be obscured are drawn with dashes. The qualitative topography of the PESs is general to other compounds of the same class, including **I**.[38]

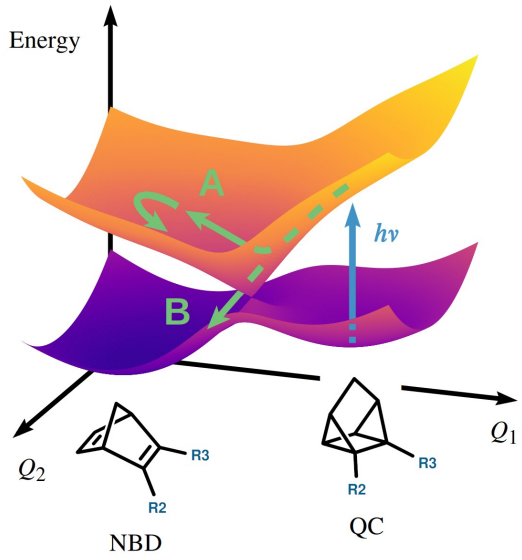

(a) QC→NBD cycloreversion

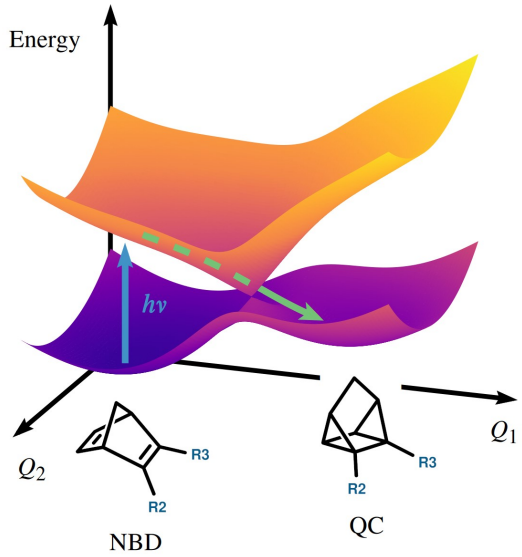

(b) NBD→QC cycloaddition

3.3 Minor Relaxation Pathways

We now move on to examine the two minor relaxation pathways which emerge in the simulations. The first is the formation of the RICT state. RICT states[83–94] are intramolecular charge

View Article Online
DOI: 10.1039/D6CP01643J

transfer excited states in which an electron is transferred from an out-of-plane π-type orbital of an aromatic moiety into an in-plane π^*-type orbital of a nitrile (–C≡N) or an ethynyl (–C≡C–) group. States of this type are also often referred to as $\pi\sigma^*$ states; in this convention, the in-plane π^*-type orbital is considered a σ^*-type orbital.[84]

Previous computational studies have indicated that RICT states adopt geometries where the participating nitrile or ethynyl group is bent instead of linear,[83–86] suggesting that the relevant carbon atom, or atoms, have changed hybridisation from sp to sp^2. Indeed, the characteristic bending of the ethynyl group is clearly seen in our simulations (see the representative trajectory shown in Figure 5 (c)). In fact, the bending of the ethynyl group was precisely what enabled the pattern recognition algorithm to identify the RICT state in the simulations. The algorithm only takes into account the time-evolution of molecular geometry – more specifically, the inverse interatomic distances. It is not provided with information on the electronic structure of the molecule. Hence, the only way it could detect the RICT state is by the tell-tale bending of the ethynyl group.

To date, there have been no time-resolved spectroscopic studies of **II** or other push-pull photoswitches which possess an ethynyl linker, meaning that there is no definitive evidence either for or against the possibility that these compounds adopt RICT states. Still, some previous studies have predicted the formation of RICT states in other molecules containing ethynyl linkers.[86–89,93] Notably, Flock and co-workers[93] investigated the photorelaxation dynamics of gas-phase diphenylacetylene (C_6H_5–C≡C–C_6H_5) with the use of time-resolved photoelectron spectroscopy (TRPES). These authors observed a transient photoelectron signal that they attributed to the RICT structure. (Note that, in Ref. 93, the RICT structure was termed the *trans-bent* structure.) Considering the findings of these studies, it seems plausible that **II** can indeed adopt a RICT state.

In the case of QC-**II**, geometry optimisations at the TDDFT-1D level of theory indicate that there are two RICT minima on the PES of state S_1; their structures are shown in Figure 8 (a) and (b). The main difference between the two RICT structures is the direction in which the ethynyl linker bends – either towards or away from the nitrile group. They are very close to one another in energy – to within around 0.01 eV, or 1 kJ/mol. (Here, we are taking into account zero-point vibrational energy corrections to total energies. We have verified that both of the two RICT structures correspond to energy minima by calculating their vibrational frequencies numerically, using analytical energy gradients.)

Being energy minima, the two RICT structures are able to temporarily trap a fraction of the excited-state population. The timescale of our simulations was, unfortunately, too short to determine the ultimate fate of all 16 trajectories which became trapped in the RICT structures, and which the pattern recognition algorithm assigned to cluster 3. One of these 16 trajectories eventually escaped from the RICT structure and underwent ring opening, while another approached an S_1/S_0 CI that is apparently unrelated to ring opening, and underwent internal conversion to the ground state. The other 14 trajectories in cluster 3 remained trapped in the RICT structure until the end of the simulation.

We were able to optimise the MECI structures that are responsible for the $S_1 \rightarrow S_0$ internal conversion processes of the RICT structures; their geometries are shown in Figure 8 (c) and (d). As might be expected, there are two MECI structures of this type; they differ from one another in the direction of the bending of the ethynyl linker.

The MECI structure that is similar in terms of geometry to RICT structure 1 (Figure 8 (c)) is higher in energy than RICT structure 1 by 0.50 eV. Meanwhile, the MECI structure that is similar to RICT structure 2 (Figure 8 (d)) is higher in energy than RICT structure 2 by 0.61 eV. These fairly large energy differences indicate that internal conversion at the two RICT-like MECI structures is an activated process. This explains why, in the relatively short NAMD simulations, we only observed one instance where the molecule underwent an $S_1 \rightarrow S_0$ hop near one of these MECI structures. (NB: the energy differences that we have given here do not include zero-point vibrational energy corrections, as these corrections cannot be defined for a MECI structure.)

The second minor relaxation pathway, associated with cluster 4, involves the breakup of the QC moiety. One of the 9 trajectories which have been assigned to this cluster is shown in Figure 5 (d). In all cases, the breakup started with the dissociation of the C1–C2 and C2–C6 bonds, which is formally a $[3 \rightarrow 2 + 1]$ cycloelimination reaction.

The subsequent dynamics of the molecule varied from one trajectory to another. In 6 trajectories, the dissociation of the C1–C2 and C2–C6 bonds was additionally followed by the dissociation of the C3–C5 bond. Interestingly, in 2 of these 6 trajectories, the molecule eventually isomerised into NBD-**II**. In other words, the photoinduced damage repaired itself spontaneously, although the molecule ended up in the NBD isomeric form. This indicates that the cleavage of the C1–C2 and C2–C6 bonds does not necessarily mean irreversible damage to the photoswitch molecule.

In order to characterise the photoproducts formed through the breakup of the QC moiety, we extracted molecular geometries from trajectories belonging to cluster 4, and used them as starting points for geometry optimisations on the PES of state S_0. We located two energy minima in this manner; their geometries are shown in Figure 8 (e) and (f). These structures are best described as two isomers of the carbene photoproduct which arises from the cleavage of the C1–C2 and the C2–C6 bonds of the QC isomer of the photoswitch. They seemingly differ from one another in molecular geometry as well as in electronic structure. In isomer 1 (see Figure 8 (e)), the non-bonding electrons are presumably localised on the carbon atom that is adjacent to the phenyl group, causing it to adopt a bent geometry. In isomer 2 (Figure 8 (f)), they appear to be localised on atom C2, and it is that atom which adopts a bent geometry. Bent geometries of the type seen in these two structures are typical of carbenes in singlet electronic states.[95–97] Isomer 2 is calculated to be slightly higher in energy than isomer 1 (by 0.06 eV, or 6 kJ/mol).

Singlet carbenes are typically highly reactive, and so the carbene photoproduct is likely able to undergo further

View Article Online
DOI: 10.1039/D6CP01643J

Fig. 8 Molecular geometries which are relevant to the minor relaxation pathways of the QC-**II** as optimised at the TDDFT-1D level of theory. Selected bond lengths are given in units of Ångström.

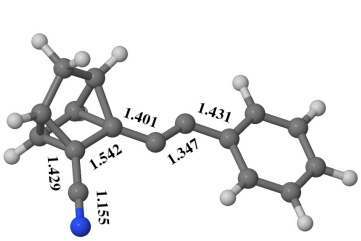

(a) RICT structure 1
(minimum on PES of state S_1)

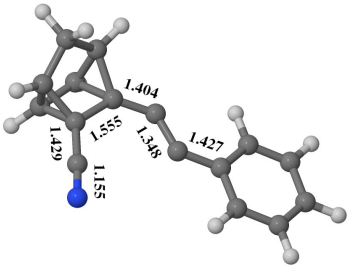

(b) RICT structure 2
(minimum on PES of state S_1)

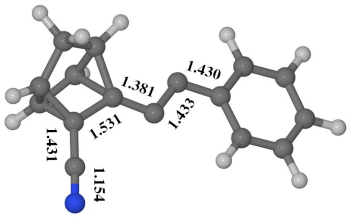

(c) RICT-like S_1/S_0 MECI structure 1
(minimum-energy point along S_1/S_0 CI seam)

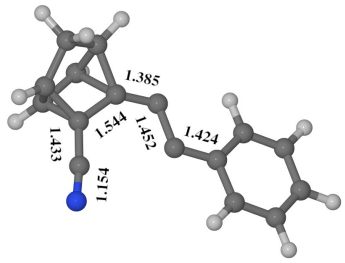

(d) RICT-like S_1/S_0 MECI structure 2
(minimum-energy point along S_1/S_0 CI seam)

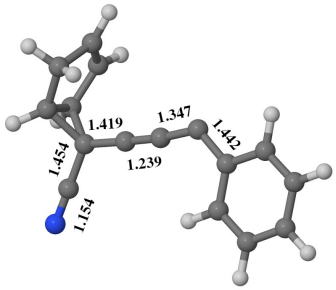

(e) carbene photoproduct, isomer 1
(minimum on PES of state S_0)

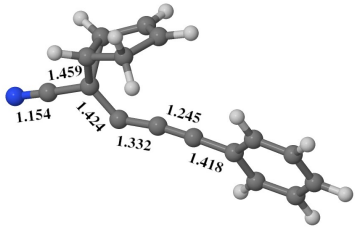

(f) carbene photoproduct, isomer 2
(minimum on PES of state S_0)

intramolecular isomerisation reactions, some of which may be irreversible, as well as intermolecular reactions with the solvent and/or with intact molecules of the photoswitch. We therefore hypothesise that the formation of the carbene photoproduct may be the first step in the UV-induced decomposition of the photoswitch.

As for the photoproduct in which the bonds C1–C2, C2–C6, and C3–C5 are all broken, we encountered convergence problems when attempting to optimise its geometry at the TDDFT-1D level. For this reason, it remains an open question whether this photoproduct corresponds to an energy minimum at the TDDFT-1D level of theory.

Nonetheless, in order to circumvent the convergence problems which arose in the TDDFT-1D calculation, we re-ran this geometry optimisation with the MRSF-TDDFT method, which in this case proved numerically stable. The computational parameters were as specified in Section S1.2.1 of the Supplementary Information. In the course of the geometry optimisation at the MRSF-TDDFT level, the molecule eventually relaxed to the NBD isomeric form. This suggests that the photoproduct with the three broken bonds does not correspond to an energy minimum, at least not according to the MRSF-TDDFT method. Rather, it appears to be associated with a broad, flat region of the PES of state S_0.

4 Conclusions

The simulation results have positive as well as negative implications. On one hand, the two photorelaxation pathways which mainly involve the opening and re-closing of the four-membered ring enable the QC isomers to undergo non-radiative deactivation without suffering damage. This is clearly a factor which contributes to photostability. On the other hand, a small fraction of photoexcited molecules undergo a breakup of the QC moiety, leading to a singlet carbene photoproduct. This is, in a sense, unsurprising, given the highly strained nature of the QC moiety. We conjecture that the resulting carbene may act as a reaction intermediate in the UV-induced decomposition of the photoswitch.

The static calculations (geometry optimisations and PES scans) reported in the Supplementary Information indicate that the breakup of the QC moiety is not limited to compound **II**, but it is also possible in compound **I**, in which the donor group is directly attached to the QC moiety. Presumably, this relaxation pathway is a general feature of the photochemistry of the QC isomers of NBD-QC photoswitches.

To the best of our knowledge, at present there is no experimental evidence for the formation of the carbene photoproduct. If this species is indeed formed, it is likely short-lived and, hence, elusive. One way to indirectly detect its formation might be to trap it with an unsaturated species (an alkene or alkyne) that is reactive towards carbenes, but is otherwise chemically and photochemically inert.[98–102] In practical terms, this might be achieved by irradiating the QC isomer of a photoswitch in an unsaturated hydrocarbon, such as cyclohexene, as solvent.

As regards the timescale of the QC→NBD photoinduced cycloreversion reaction, in our simulations the ring dynamics is largely complete within the simulation time of 750 fs. More precisely, the exact timescale of ring opening depends on whether

View Article Online
DOI: 10.1039/D6CP01643J

we take into account the re-closing of the ring in some of the simulated trajectories, but in any case, the ring opening and re-closing processes take place within a few hundreds of femtoseconds of the initial photoexcitation. This is considerably shorter than the timescale of ca. 62 ps reported by Alex et al.[40] for QC-**IV**. We hypothesise that the longer timescale does not correspond to ring opening per se. Rather, it might be the lifetime of an excited-state species that is formed after the photoexcitation of QC-**IV**.

Conflicts of Interest

There are no conflicts of interest to declare.

Data Availability

Data for this article are available at the repository Zenodo as Ref. 73.

Acknowledgements

M. A. K. thanks Prof. Dr John Herbert for a helpful discussion on the convergence behaviour of TDDFT-1D.

This work was supported by the National Science Center (Poland) under the OPUS grant no. 2025/57/B/ST4/01066. B. D. thanks the Swedish Research Council (Grant No. 2019-03664), the Olle Engkvist Foundation (Grant No. 204-0183) and the Carl Trygger Foundation (Grant No. CTS 24:3446). M. A. K. thanks the Alexander von Humboldt Foundation for the award of a research fellowship.

The simulations reported in this article were carried out with the use of the computational resources kindly provided to the authors by the Wrocław Centre for Networking and Supercomputing (WCSS, https://wcss.pl), the Centre of Informatics of the Tricity Academic Supercomputer and Network (CI TASK, https://task.gda.pl), the Poznań Supercomputing and Networking Center affiliated to the Institute of Bioorganic Chemistry of the Polish Academy of Sciences (PCSS, https://www.pcss.pl), and the Interdisciplinary Centre for Mathematical and Computational Modelling, University of Warsaw (ICM UW, https://icm.edu.pl). The authors gratefully acknowledge the generous support from these agencies.

References

1 H. Ritchie, P. Rosado and M. Roser, *Energy Production and Consumption*, `https://ourworldindata.org/energy-production-consumption`.
2 V. A. Bren', A. D. Dubonosov, V. I. Minkin and V. A. Chernoivanov, *Russ. Chem. Rev. (Engl. Transl.)*, 1991, **60**, 451–469.
3 A. Lennartson, A. Roffey and K. Moth-Poulsen, *Tetrahedron Lett.*, 2015, **56**, 1457–1465.
4 C.-L. Sun, C. Wang and R. Boulatov, *ChemPhotoChem*, 2019, **3**, 268–283.
5 A. Gimenez-Gomez, L. Magson, B. Peñin, N. Sanosa, J. Soilán, R. Losantos and D. Sampedro, *Photochem*, 2022, **2**, 694–716.
6 Z. Wang, H. Hölzel and K. Moth-Poulsen, *Chem. Soc. Rev.*, 2022, **51**, 7313–7326.
7 A. Giménez-Gómez, L. Magson, C. Merino-Robledillo, S. Hernáez-Troya, N. Sanosa, D. Sampedro and I. Funes-Ardoiz, *React. Chem. Eng.*, 2024, **9**, 1629–1640.
8 R. J. Salthouse and K. Moth-Poulsen, *J. Mater. Chem. A*, 2024, **12**, 3180–3208.
9 A. D. Dubonosov, V. A. Bren and V. A. Chernoivanov, *Russ. Chem. Rev.*, 2002, 917–927.
10 J. Orrego-Hernández, A. Dreos and K. Moth-Poulsen, *Acc. Chem. Res.*, 2020, **53**, 1478–1487.
11 F. Hemauer, H.-P. Steinrück and C. Papp, *ChemPhysChem*, 2024, **25**, e202300806.
12 M. Quant, A. Lennartson, A. Dreos, M. Kuisma, P. Erhart, K. Börjesson and K. Moth-Poulsen, *Chem. Eur. J.*, 2016, **22**, 13265–13274.
13 M. Mansø, A. U. Petersen, Z. Wang, P. Erhart, M. B. Nielsen and K. Moth-Poulsen, *Nat. Commun.*, 2018, **9**, 1945.
14 M. Mansø, B. E. Tebikachew, K. Moth-Poulsen and M. B. Nielsen, *Org. Biomol. Chem.*, 2018, **16**, 5585–5590.
15 M. Jevric, A. U. Petersen, M. Mansø, S. Kumar Singh, Z. Wang, A. Dreos, C. Sumby, M. B. Nielsen, K. Börjesson, P. Erhart *et al.*, *Chem. Eur. J.*, 2018, **24**, 12767–12772.
16 M. Quant, A. Hamrin, A. Lennartson, P. Erhart and K. Moth-Poulsen, *J. Phys. Chem. C*, 2019, **123**, 7081–7087.
17 Z. Wang, A. Roffey, R. Losantos, A. Lennartson, M. Jevric, A. U. Petersen, M. Quant, A. Dreos, X. Wen, D. Sampedro *et al.*, *Energy Environ. Sci.*, 2019, **12**, 187–193.
18 J. Orrego-Hernández, H. Hölzel, M. Quant, Z. Wang and K. Moth-Poulsen, *Eur. J. Org. Chem.*, 2021, **2021**, 5337–5342.
19 A. E. Hillers-Bendtsen, Y. Todarwal, P. Norman and K. V. Mikkelsen, *J. Phys. Chem. A*, 2024, **128**, 2602–2610.
20 D. Krappmann and A. Hirsch, *Chem. Eur. J.*, 2024, **30**, e202401391.
21 R. R. Weber, C. N. Stindt, A. M. van der Harten and B. L. Feringa, *Chem. Eur. J.*, 2024, **30**, e202400482.
22 A. S. Aslam, L. M. Muhammad, A. Erbs Hillers-Bendtsen, K. V. Mikkelsen and K. Moth-Poulsen, *Chem. Eur. J.*, 2024, **30**, e202401430.
23 U. Bauer, L. Fromm, C. Weiß, P. Bachmann, F. Spath, F. Dull, J. Steinhauer, W. Hieringer, A. Görling, A. Hirsch *et al.*, *J. Phys. Chem. C*, 2018, **123**, 7654–7664.
24 E. Franz, N. Oberhof, D. Krappmann, N. Baggi, Z. Hussain, K. Moth-Poulsen, H. Hölzel, A. Hirsch, A. Dreuw, O. Brummel *et al.*, *Chem. Eur. J.*, 2025, **31**, e02294.
25 F. Waidhas, M. Jevric, L. Fromm, M. Bertram, A. Görling, K. Moth-Poulsen, O. Brummel and J. Libuda, *Nano Energy*, 2019, **63**, 103872.
26 E. Franz, D. Krappmann, L. Fromm, T. Luchs, A. Görling, A. Hirsch, O. Brummel and J. Libuda, *ChemSusChem*, 2022, **15**, e202201483.
27 W. Zika, A. Leng, R. Weiß, S. Pintér, C. M. Schüßlbauer, T. Clark, A. Hirsch and D. M. Guldi, *Chem. Sci.*, 2023, **14**, 11096–11104.

View Article Online
DOI: 10.1039/D6CP01643J

28 S. Pintér, N. M. Strassner, D. Krappmann, E. J. Schulze and A. Hirsch, *Chem. Eur. J.*, 2025, **31**, e02610.
29 A. S. Aslam, M. Shamsabadi, R. J. Salthouse, J. Andréasson and K. Moth-Poulsen, *ChemSusChem*, 2025, **18**, e202501005.
30 A. U. Petersen, A. I. Hofmann, M. Fillols, M. Mansø, M. Jevric, Z. Wang, C. J. Sumby, C. Müller and K. Moth-Poulsen, *Adv. Sci.*, 2019, **6**, 1900367.
31 Z. Wang, H. Hölzel, L. Fernandez, A. S. Aslam, P. Baronas, J. Orrego-Hernández, S. Ghasemi, M. Campoy-Quiles and K. Moth-Poulsen, *Joule*, 2024, **8**, 2607–2622.
32 Z. Wang, J. Udmark, K. Börjesson, R. Rodrigues, A. Roffey, M. Abrahamsson, M. B. Nielsen and K. Moth-Poulsen, *ChemSusChem*, 2017, **10**, 3049–3055.
33 Z. Wang, R. Losantos, D. Sampedro, M.-a. Morikawa, K. Börjesson, N. Kimizuka and K. Moth-Poulsen, *J. Mater. Chem. A*, 2019, **7**, 15042–15047.
34 F. Coppola, M. Nucci, M. Marazzi, D. Rocca and M. Pastore, *ChemPhotoChem*, 2023, **7**, e202200214.
35 F. J. Hernández, J. M. Cox, J. Li, R. Crespo-Otero and S. A. Lopez, *J. Org. Chem.*, 2023, **88**, 5311–5320.
36 J. C. Cooper and A. Kirrander, *Phys. Chem. Chem. Phys.*, 2025, **27**, 3089–3101.
37 J. Cooper, C. Brown, J. Kára and A. Kirrander, *J. Chem. Phys.*, 2025, **162**, 094102.
38 M. A. Kochman and B. Durbeej, *J. Phys. Chem. Lett.*, 2025, **16**, 4315–4325.
39 F. J. Hernández, J. M. Cox, J. Li, S. Lopez and R. Crespo-Otero, *Chem. Sci.*, 2026, 7157–7170.
40 W. Alex, P. Lorenz, C. Henkel, T. Clark, A. Hirsch and D. M. Guldi, *J. Am. Chem. Soc.*, 2021, **144**, 153–162.
41 K. D. Borne, J. C. Cooper, M. N. Ashfold, J. Bachmann, S. Bhattacharyya, R. Boll, M. Bonanomi, M. Bosch, C. Callegari, M. Centurion *et al.*, *Nat. Chem.*, 2024, **16**, 499–505.
42 L. Fei, H. Hölzel, Z. Wang, A. E. Hillers-Bendtsen, A. S. Aslam, M. Shamsabadi, J. Tan, K. V. Mikkelsen, C. Wang and K. Moth-Poulsen, *Chem. Sci.*, 2024, **15**, 18179–18186.
43 F. Agostini and B. F. Curchod, *WIREs Comput. Mol. Sci.*, 2019, **9**, e1417.
44 T. R. Nelson, A. J. White, J. A. Bjorgaard, A. E. Sifain, Y. Zhang, B. Nebgen, S. Fernandez-Alberti, D. Mozyrsky, A. E. Roitberg and S. Tretiak, *Chem. Rev.*, 2020, **120**, 2215–2287.
45 S. Battaglia and R. Lindh, *J. Chem. Phys.*, 2021, **154**, 034102.
46 K. Mizuno, N. Ichinose and Y. Yoshimi, *J. Photochem. Photobiol. C*, 2000, **1**, 167–193.
47 E. Tapavicza, I. Tavernelli, U. Rothlisberger, C. Filippi and M. E. Casida, *J. Chem. Phys.*, 2008, **129**, 124108.
48 M. S. Robinson, M. Niebuhr, F. Lever, D. Mayer, J. Metje and M. Gühr, *Chem. Eur. J.*, 2021, **27**, 11418–11427.
49 J. C. Tully and R. K. Preston, *J. Chem. Phys.*, 1971, **55**, 562–572.
50 J. C. Tully, *J. Chem. Phys.*, 1990, **93**, 1061–1071.
51 S. Hammes-Schiffer and J. C. Tully, *J. Chem. Phys.*, 1994, **101**, 4657–4667.
52 G. Granucci and M. Persico, *J. Chem. Phys.*, 2007, **126**, 134114.
53 Y. Shao, M. Head-Gordon and A. I. Krylov, *J. Chem. Phys.*, 2003, **118**, 4807–4818.
54 S. Lee, M. Filatov, S. Lee and C. H. Choi, *J. Chem. Phys.*, 2018, **149**, 104101.
55 D. Casanova and A. I. Krylov, *Phys. Chem. Chem. Phys.*, 2020, **22**, 4326–4342.
56 Y. Horbatenko, S. Sadiq, S. Lee, M. Filatov and C. H. Choi, *J. Chem. Theory Comput.*, 2021, **17**, 848–859.
57 J. M. Herbert and A. Mandal, in *Time-dependent density functional theory*, Jenny Stanford Publishing, 2022, pp. 361–404.
58 W. Park, K. Komarov, S. Lee and C. H. Choi, *J. Phys. Chem. Lett.*, 2023, **14**, 8896–8908.
59 M. Filatov, V. Mironov and E. Kraka, *J. Comput. Chem.*, 2024, **45**, 1033–1045.
60 J. Janoš, A. J. Orr-Ewing, B. F. E. Curchod and P. Slavíček, *arXiv*, 2026, preprint, DOI: 10.48550/arXiv.2604.09230.
61 H.-H. Teh and J. E. Subotnik, *J. Phys. Chem. Lett.*, 2019, **10**, 3426–3432.
62 H.-H. Teh and J. E. Subotnik, *J. Chem. Phys.*, 2020, **153**, 244110.
63 V. Athavale, H.-H. Teh and J. E. Subotnik, *J. Chem. Phys.*, 2021, **155**, 154105.
64 V. Athavale, H.-H. Teh, Y. Shao and J. Subotnik, *J. Chem. Phys.*, 2022, **157**, 244110.
65 A. I. Krylov and P. M. W. Gill, *WIREs Comput. Mol. Sci.*, 2013, **3**, 317–326.
66 Y. Shao, Z. Gan, E. Epifanovsky, A. T. Gilbert, M. Wormit, J. Kussmann, A. W. Lange, A. Behn, J. Deng, X. Feng, D. Ghosh, M. Goldey, P. R. Horn, L. D. Jacobson, I. Kaliman, R. Z. Khaliullin, T. Kuś, A. Landau, J. Liu, E. I. Proynov, Y. M. Rhee, R. M. Richard, M. A. Rohrdanz, R. P. Steele, E. J. Sundstrom, H. L. Woodcock, P. M. Zimmerman, D. Zuev, B. Albrecht, E. Alguire, B. Austin, G. J. O. Beran, Y. A. Bernard, E. Berquist, K. Brandhorst, K. B. Bravaya, S. T. Brown, D. Casanova, C.-M. Chang, Y. Chen, S. H. Chien, K. D. Closser, D. L. Crittenden, M. Diedenhofen, R. A. DiStasio, H. Do, A. D. Dutoi, R. G. Edgar, S. Fatehi, L. Fusti-Molnar, A. Ghysels, A. Golubeva-Zadorozhnaya, J. Gomes, M. W. Hanson-Heine, P. H. Harbach, A. W. Hauser, E. G. Hohenstein, Z. C. Holden, T.-C. Jagau, H. Ji, B. Kaduk, K. Khistyaev, J. Kim, J. Kim, R. A. King, P. Klunzinger, D. Kosenkov, T. Kowalczyk, C. M. Krauter, K. U. Lao, A. D. Laurent, K. V. Lawler, S. V. Levchenko, C. Y. Lin, F. Liu, E. Livshits, R. C. Lochan, A. Luenser, P. Manohar, S. F. Manzer, S.-P. Mao, N. Mardirossian, A. V. Marenich, S. A. Maurer, N. J. Mayhall, E. Neuscamman, C. M. Oana, R. Olivares-Amaya, D. P. O'Neill, J. A. Parkhill, T. M. Perrine, R. Peverati, A. Prociuk, D. R. Rehn, E. Rosta, N. J. Russ, S. M.

View Article Online
DOI: 10.1039/D6CP01643J

Sharada, S. Sharma, D. W. Small, A. Sodt, T. Stein, D. Stück, Y.-C. Su, A. J. Thom, T. Tsuchimochi, V. Vanovschi, L. Vogt, O. Vydrov, T. Wang, M. A. Watson, J. Wenzel, A. White, C. F. Williams, J. Yang, S. Yeganeh, S. R. Yost, Z.-Q. You, I. Y. Zhang, X. Zhang, Y. Zhao, B. R. Brooks, G. K. Chan, D. M. Chipman, C. J. Cramer, W. A. Goddard, M. S. Gordon, W. J. Hehre, A. Klamt, H. F. Schaefer, M. W. Schmidt, C. D. Sherrill, D. G. Truhlar, A. Warshel, X. Xu, A. Aspuru-Guzik, R. Baer, A. T. Bell, N. A. Besley, J.-D. Chai, A. Dreuw, B. D. Dunietz, T. R. Furlani, S. R. Gwaltney, C.-P. Hsu, Y. Jung, J. Kong, D. S. Lambrecht, W. Liang, C. Ochsenfeld, V. A. Rassolov, L. V. Slipchenko, J. E. Subotnik, T. Van Voorhis, J. M. Herbert, A. I. Krylov, P. M. Gill and M. Head-Gordon, *Mol. Phys.*, 2015, **113**, 184–215.

67 T. Yanai, D. P. Tew and N. C. Handy, *Chem. Phys. Lett.*, 2004, **393**, 51–57.

68 F. Weigend and R. Ahlrichs, *Phys. Chem. Chem. Phys.*, 2005, **7**, 3297–3305.

69 P. G. Szalay, T. Watson, A. Perera, V. Lotrich, G. Fogarasi and R. J. Bartlett, *J. Phys. Chem. A*, 2012, **116**, 8851–8860.

70 T. Shiozaki, W. Győrffy, P. Celani and H.-J. Werner, *J. Chem. Phys.*, 2011, **135**, 081106.

71 E. B. Wilson, *J. Am. Stat. Assoc.*, 1927, **22**, 209–212.

72 S. Wallis, *J. Quant. Linguist.*, 2013, **20**, 178–208.

73 B. Durbeej, S. Pintér, A. Hirsch and M. A. Kochman, *Dataset on the Photochemistry of the Energy-Storing Isomer of a Norbornadiene-Based Molecular Switch. Zenodo* **2026**, `https://doi.org/10.5281/zenodo.19664763`.

74 M. Rupp, A. Tkatchenko, K.-R. Müller and O. A. Von Lilienfeld, *Phys. Rev. Lett.*, 2012, **108**, 058301.

75 M. Rupp, *Int. J. Quantum Chem.*, 2015, **115**, 1058–1073.

76 R. Bellman and R. Kalaba, *IRE Transactions on Automatic Control*, 1959, **4**, 1–9.

77 P. Senin, *Dynamic time warping algorithm review*, 2008, `https://seninp.github.io/assets/pubs/senin_dtw_litreview_2008.pdf`.

78 C. F. Jekel, G. Venter, M. P. Venter, N. Stander and R. T. Haftka, *Int. J. Mater. Form.*, 2019, **12**, 355–378.

79 *similarity_measures*, `https://github.com/cjekel/similarity_measures`.

80 J. H. Ward Jr, *J. Am. Stat. Assoc.*, 1963, **58**, 236–244.

81 F. Murtagh and P. Legendre, *J. Classif.*, 2014, **31**, 274–295.

82 P. Virtanen, R. Gommers, T. E. Oliphant, M. Haberland, T. Reddy, D. Cournapeau, E. Burovski, P. Peterson, W. Weckesser, J. Bright *et al.*, *Nat. Methods*, 2020, **17**, 261–272.

83 F. D. Lewis and B. Holman III, *J. Phys. Chem.*, 1980, **84**, 2326–2328.

84 A. L. Sobolewski and W. Domcke, *Chem. Phys. Lett.*, 1996, **250**, 428–436.

85 A. L. Sobolewski and W. Domcke, *Chem. Phys. Lett.*, 1996, **259**, 119–127.

86 A. L. Sobolewski and W. Domcke, *J. Photochem. Photobiol., A: Chem.*, 1997, **105**, 325–328.

87 M. Z. Zgierski and E. C. Lim, *Chem. Phys. Lett.*, 2004, **387**, 352–355.

88 T. Fujiwara, J.-K. Lee, M. Z. Zgierski and E. C. Lim, *Phys. Chem. Chem. Phys.*, 2009, **11**, 2475–2479.

89 J.-K. Lee, T. Fujiwara, W. G. Kofron, M. Z. Zgierski and E. C. Lim, *J. Chem. Phys.*, 2008, **128**, 164512.

90 P. B. Coto, L. Serrano-Andrés, T. Gustavsson, T. Fujiwara and E. C. Lim, *Phys. Chem. Chem. Phys.*, 2011, **13**, 15182–15188.

91 I. Georgieva, A. J. A. Aquino, F. Plasser, N. Trendafilova, A. Köhn and H. Lischka, *J. Phys. Chem. A*, 2015, **119**, 6232–6243.

92 B. Dereka, D. Svechkarev, A. Rosspeintner, M. Tromayer, R. Liska, A. M. Mohs and E. Vauthey, *J. Am. Chem. Soc.*, 2017, **139**, 16885–16893.

93 M. Flock, L. Bosse, D. Kaiser, B. Engels and I. Fischer, *Phys. Chem. Chem. Phys.*, 2019, **21**, 13157–13164.

94 Z. Lou, X. Zhou, Z. Tang and P. Zhou, *J. Phys. Chem. B*, 2020, **124**, 4564–4572.

95 C. D. Sherrill, M. L. Leininger, T. J. Van Huis and H. F. Schaefer III, *J. Chem. Phys.*, 1998, **108**, 1040–1049.

96 H. L. Woodcock, D. Moran, B. R. Brooks, P. v. R. Schleyer and H. F. Schaefer, *J. Am. Chem. Soc.*, 2007, **129**, 3763–3770.

97 D. J. Goebbert, K. Pichugin, D. Khuseynov, P. G. Wenthold and A. Sanov, *J. Chem. Phys.*, 2010, **132**, 224301.

98 G. W. Griffin, *Angew. Chem. Int. Ed. Engl.*, 1971, **10**, 537–547.

99 T. Savino, K. Kanakarajan and M. Platz, *J. Org. Chem.*, 1986, **51**, 1305–1309.

100 M. Jones Jr. and R. A. Moss, in *Singlet Carbenes*, John Wiley & Sons, Ltd, 2003, ch. 7, pp. 273–328.

101 S. Jana, C. Pei, C. Empel and R. M. Koenigs, *Angew. Chem. Int. Ed.*, 2021, **60**, 13271–13279.

102 B. Sawyer, J. L. Peltier and R. Jazzar, *Chem. Eur. J.*, 2025, **31**, e202501600.

View Article Online
DOI: 10.1039/D6CP01643J

Data Availability Statement for Manuscript

UV Photochemistry of the Energy-Storing Isomer of a Norbornadiene-Based Molecular Switch: Ring Opening, Rehybridised Intramolecular Charge Transfer, and Isomerisation into a Carbene Photoproduct

by Bo Durbeej, Simone Pintér, Andreas Hirsch, and Michał Andrzej Kochman

The following data for this article are available at the repository Zenodo at https://doi.org/10.5281/zenodo.18888657

1. Program for NAMD Simulations with the TDDFT-1D Method

2. NAMD Trajectories of the Photorelaxation Process of the Quadricyclane Isomer of a Norbornadiene-Based Molecular Switch

3. Animations of Simulated Trajectories

4. Input and Output Files for the Electronic Structure Calculations Reported in our Study